Stepwise Hapticity Changes in Sequential One-Electron Redox Reactions of Indenyl-Molybdenum Complexes: Combined Electrochemical, ESR, X-ray, and Theoretical Studies

Michael E. Stoll,[†] Paola Belanzoni,[‡] Maria J. Calhorda,*[,§,||] Michael G. B. Drew,[⊥] Vitor Félix,[▽] William E. Geiger,*[,†] Carla A. Gamelas,[§,#] Isabel S. Gonçalves,[§,▽] Carlos C. Romão,*[,§] and Luís F. Veiros[×]

Contribution from the Department of Chemistry, University of Vermont, Cook Physical Science Building, Burlington, Vermont 05405-0125, Dipartimento di Chimica, Università di Perugia, via Elce di Sotto 8, 06123 Perugia, Italy, Instituto de Tecnologia Quimíca e Biológica, Quinta do Marquês, EAN, Apt 127, 2780-151 Oeiras, Portugal, Departamento de Química e Bioquímica, Faculdade de Ciências, Universidade de Lisboa, 1700 Lisboa Codex, Portugal, Department of Chemistry, University of Reading, Whiteknights, Reading, RG6 6AD, U.K., Departmento de Química, Universidade de Aveiro, 3810-193 Aveiro, Portugal, Escola Superior de Tecnologia, Instituto Politécnico de Setúbal, 2900 Setúbal, Portugal, and Centro de Química Estrutural, Instituto Superior Técnico, 1096 Lisboa Codex, Portugal

Received April 19, 2001

Abstract: Reduction of the dication $[(\eta^5\text{-Ind})(\text{Cp})\text{Mo}\{\text{P}(\text{OMe})_3\}_2]^{2+}$ ($\mathbf{1}^{2+}$) and oxidation of the neutral complex $(\eta^3\text{-Ind})(\text{Cp})\text{Mo}\{\text{P}(\text{OMe})_3\}_2$ (**1**) proceed through a one-electron intermediate, $\mathbf{1}^+$. The structures of $\mathbf{1}^{2+}$ and **1** have been determined by X-ray diffraction studies, which show the slip-fold distortion angle, Ω, of the indenyl ring increasing from 4.1° in $\mathbf{1}^{2+}$ to 21.7° in **1**. Cyclic voltammetry and bulk electrolysis were employed to define the thermodynamics and heterogeneous charge-transfer kinetics of reactions $\mathbf{1}^{2+} + e^- \rightleftharpoons \mathbf{1}^+$ and $\mathbf{1}^+ + e^- \rightleftharpoons \mathbf{1}$: $\Delta E_{1/2} = 113$ mV in CH_3CN and 219 mV in CH_2Cl_2/0.1 M $[NBu_4][PF_6]$; $k_s = 0.4$ cm s^{-1} for $\mathbf{1}^{2+}/\mathbf{1}^+$ couple, 1.0 cm s^{-1} for $\mathbf{1}^+/\mathbf{1}$ couple in CH_3CN. ESR spectra of $\mathbf{1}^+$ displayed a surprisingly large hyperfine splitting (7.4×10^{-4} cm^{-1}) from a single ^{1}H nucleus, and spectra of the partially deuterated indenyl analogue confirmed assignment of a_H to the H(2) proton of the indenyl ring. The related η^5 18-electron complexes $[(\eta^5\text{-Ind})(\text{Cp})\text{Mo}(\text{dppe})]^{2+}$ ($\mathbf{2}^{2+}$) (dppe = diphenylphosphinoethane) and $(\eta^5\text{-Ind})(\text{Cp})\text{Mo}(\text{CN})_2$ (**3**) may also be reduced in two successive one-electron steps; ESR spectra of the radicals $\mathbf{2}^+$ and $\mathbf{3}^-$ showed a similarly large $a_{H(2)}$ (8.7×10^{-4} and 6.4×10^{-4} cm^{-1}, respectively). Molecular orbital calculations (density functional theory, DFT, and extended Hückel, EH) predict metal-indenyl bonding in $\mathbf{1}^+$ that is approximately *midway* between that of the η^5 and η^3 hapticities (e.g., $\Omega = 11.4°$). DFT results show that the large value of $a_{H(2)}$ arises from polarization of the indenyl-H(2) by both inner-sphere orbitals and the singly occupied molecular orbital (SOMO) of $\mathbf{1}^+$. The measured k_s values are consistent with only minor inner-sphere reorganizational energies being necessary for the electron-transfer reactions, showing that a full η^5/η^3 hapticity change may require only small inner-sphere reorganization energies when concomitant with a pair of *stepwise* one-electron-transfer processes. The indenyl ligand in $\mathbf{1}^+$ is best described as donating approximately four π-electrons to Mo by combining a traditional η^3 linkage with two "half-strength" Mo−C bonds.

Introduction

The hapticity of a polyolefin ligand often exerts a dominant influence on the reactivity of its metal complexes.[1] One such ligand, namely the indenyl (Ind) anion, is of special interest[2] owing to its analogy to the common and important cyclopentadienyl (Cp) anion. The propensity of the former to undergo slip-fold distortion from a pentahapto (η^5) to a trihapto (η^3) bonding mode[3] accounts for its being viewed as a polyolefin ligand in the "facile slippage" limit, useful in probing how ring slippage may affect substitution reactions.[4] Within the context of organometallic radical chemistry, efforts have been made to determine how the slip-fold distortion is affected by stepwise *one-electron* transfer reactions. Definitive answers through X-ray structures have been obtained, however, only for bisindenyl-metal complexes.[5,6] Marder and co-workers[5] traced the effects

[†] University of Vermont.
[‡] Università di Perugia.
[§] Instituto de Tecnologia Quimíca e Biológica.
[||] Universidade de Lisboa.
[⊥] University of Reading.
[▽] Universidade de Aveiro.
[#] Instituto Politécnico de Setúbal.
[×] Instituto Superior Técnico.

(1) Collman, J. P.; Hegedus, L. S.; Norton, J. R.; Finke, R. G. *Principles and Applications of Organotransition Metal Chemistry*; University Science Books: Mill Valley, CA, 1987; pp 255−259.
(2) (a) O'Connor, J. M.; Casey, C. P. *Chem. Rev.* **1987**, *87*, 307. (b) Veiros, L. F. *Organometallics* **2000**, *19*, 3127.
(3) (a) Rerek, M. E.; Ji, L.-N.; Basolo, F. *J. Chem. Soc., Chem. Commun.* **1983**, 1208. (b) Ji, L.-N.; Rerek, M. E.; Basolo, F. *Organometallics* **1984**, *3*, 740. (c) Recent review: Veiros, L. F. *Organometallics* **2000**, *19*, 3127.
(4) See, for example: Pevear, K. A.; Banaszak Holl, M. M.; Carpenter, G. B.; Rieger, A. L.; Rieger, P. H.; Sweigart, D. A. *Organometallics* **1995**, *14*, 512.
(5) Westcott, S. A.; Kakkar, A. K.; Stringer, G.; Taylor, N. J.; Marder, T. B. *J. Organomet. Chem.* **1990**, *394*, 777.
(6) Kowaleski, R. M.; Rheingold, A. L.; Trogler, W. C.; Basolo, F. *J. Am. Chem. Soc.* **1986**, *108*, 2460.

10.1021/ja0109951 CCC: $20.00
Published on Web 10/06/2001

of added electrons on the structures of sandwich complexes $(Ind)_2M$ (M = Fe, Co, Ni) and found *gradual* distortion of the indenyl ring away from the pentahapto bonding mode as the number of electrons increased. Also, the sandwich derivative $(Ind)_2V(CO)_2$ has been shown to possess one η^3 ring and one slightly distorted η^5 ring, resulting in an odd-electron compound having essentially a 17-electron metal.[6,7]

In contrast, well-designed efforts to probe the η^5 versus η^3 ligand hapticity of odd-electron complexes possessing a *single* indenyl ring, in which ring slippage is less likely to be divided between two π-ligands, have given more ambiguous conclusions.[4,8,9] The radicals have been generated through one-electron reductions of 18-electron precursors displaying pentahapto-indenyl bonding. Complexes $[(\eta^5\text{-Ind})Fe(CO)_3]^+$ (**4**$^+$),[4] (η^5-Ind)-$Mn(CO)_3$ (**5**),[8] and (η^5-Ind)Rh(COD) (**6**) (COD = cyclooctadiene)[9] may each be reduced in two successive one-electron stages (Eq 1), first to the radicals Red(1) (**4**, **5**$^-$, or **6**$^-$) and then to Red(2). Owing to limitations in the lifetimes and/or

$$\text{Ox} \overset{E_{1/2}(1),\, k_s(1)}{\rightleftharpoons} \text{Red(1)} \overset{E_{1/2}(2),\, k_s(2)}{\rightleftharpoons} \text{Red(2)} \qquad (1)$$

spectral properties of Red(1), arguments about the indenyl hapticities of the radicals have been largely restricted to assessment of the electrochemical properties of the two redox couples. Because the electrochemical thermodynamics and kinetics may *under some circumstances*[10,11] be influenced by molecular structure changes, voltammetry may be used, in principle, to probe whether the η^5 to η^3 indenyl ring slippage occurs during the first or second redox process of Eq 1. This approach utilizes the often easily measured $\Delta E_{1/2}$ values of the couples [$\Delta E_{1/2} = E_{1/2}(1) - E_{1/2}(2)$] and the less frequently measured heterogeneous electron-transfer kinetic (k_s) values and charge-transfer (α) parameters of the couples.[12]

Some of the constraints in using the electrochemical approach have been previously discussed.[9,11,13] Conclusions about slip-fold distortions that are based on the $\Delta E_{1/2}$ values measured for a single complex are particularly arguable, because $\Delta E_{1/2}$ may also be sensitive to metal−ligand electronic effects and to experimental measurement factors such as solvation and ion pairing (this is further examined in the Discussion section).

18-Electron complexes of the type $[(\eta^5\text{-Ind})(Cp)ML_2]^{2+}$ and $(\eta^3\text{-Ind})(Cp)ML_2$ (M = Mo, W; L = CO, PR_3) are part of a sufficiently large group of analogues[14] to allow the first systematic study of how slip-fold distortions affect electrochemical properties. Preliminary voltammetric data have been reported on several compounds in this series,[15] and the present paper amplifies those results for several systems known to undergo indenyl slip-fold changes when two electrons are gained or lost. The structures of the one-electron intermediates were evaluated through density functional theory (DFT) calculations.

Voltammetric and ESR results were appraised in light of the degree of DFT-calculated and X-ray-determined slip-fold changes in the two one-electron steps. It is found that the first and second one-electron reductions of $[(\eta^5\text{-Ind})(Cp)Mo\{P(OMe)_3\}_2]^{2+}$ (**1**$^{2+}$) [or the two corresponding oxidations of $(\eta^3\text{-Ind})(Cp)Mo\{P(OMe)_3\}_2$ (**1**)] give rise to *successive* changes in the degree of the slip-fold bends, with **1**$^+$ having a structure approximately *midway* between the two extremes expected for structures having formal 17-electron versus 19-electron metals. Although the value of $k_s(1)$ was in each case less than $k_s(2)$, both electron-transfer rates are relatively large, showing that overall η^5/η^3 indenyl-metal hapticity changes may occur with low internal rearrangement energies if the structural changes are spread out over two one-electron processes.

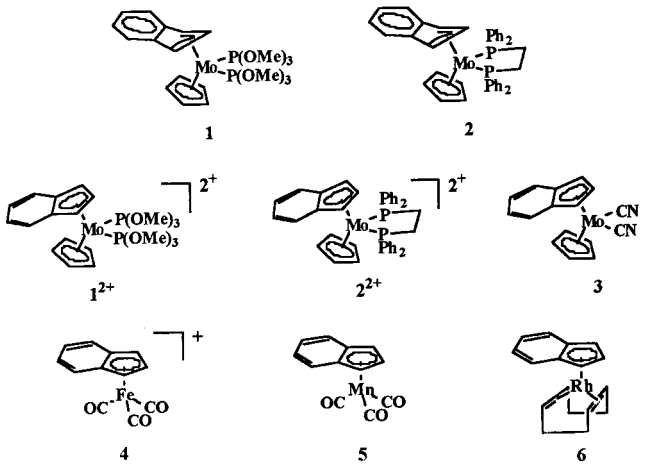

Results

Preparation and Structures. Complexes **1** and **1**$^{2+}$ were prepared following the method previously reported for $(\eta^3\text{-Ind})(Cp)Mo(dppe)$ (**2**) and $[(\eta^5\text{-Ind})(Cp)Mo(dppe)]^{2+}$ (**2**$^{2+}$).[15]

Reaction of $[(\eta^5\text{-Ind})(Cp)Mo(NCMe)_2]^{2+}$ with excess $P(OMe)_3$ in CH_2Cl_2/NMF gives the dication $[(\eta^5\text{-Ind})(Cp)Mo\{P(OMe)_3\}_2]^{2+}$ (**1**$^{2+}$) isolated as the BF_4^- salt. The ^{1}H NMR indicates the η^5 coordination of the indenyl with resonances similar to those observed for **2**$^{2+}$ and its analogue $[(\eta^5\text{-Ind})(Cp)Mo(PMe_3)_2]^{2+}$.[15] Coupling of the two P atoms to H(1,3), H(2), and the Cp ring protons is observed. The reaction of **1**$^{2+}$ with cobaltocene in a suspension of CH_3CN gives the neutral, hexane soluble $(\eta^3\text{-Ind})(Cp)Mo\{P(OMe)_3\}_2$ (**1**). This compound has been previously obtained by less obvious routes.[14e,f]

The ^{1}H NMR spectrum of **1** in C_6D_6 confirms the expected η^3 coordination with the H(1,3) resonance (a multiplet at δ 3.90−3.87 ppm) and the H(5−8) resonances (a multiplet at δ 6.56−6.50 ppm) shifted upfield and the H(2) resonance (a multiplet at δ 7.20−7.17 ppm) shifted downfield, relative to their usual positions in the η^5 coordination mode. The broad peak at δ 4.58 ppm assigned to Cp protons appears shifted upfield as observed in similar (ring-slipped-indenyl)Cp compounds.[14,15] These structural assignments were confirmed by X-ray analysis of both **1** and **1**$^{2+}$ (vide infra). These compounds, therefore, behave quite similarly to **2** and **2**$^{2+}$, in which X-ray analysis had also confirmed that the indenyl ligand goes from the η^3 to η^5 coordination modes as **2** undergoes 2-electron

(7) Miller, G. A.; Therien, M. J.; Trogler, W. C. *J. Organomet. Chem.* **1990**, *383*, 271.
(8) Lee, S.; Lovelace, S. R.; Cooper, N. J. *Organometallics* **1995**, *14*, 1974.
(9) Amatore, C.; Ceccon, A.; Santi, S.; Verpeaux, J.-N. *Chem.—Eur. J.* **1997**, *3*, 279.
(10) Geiger, W. E. *Progress in Inorganic Chemistry*; Lippard, S. J., Ed.; John Wiley: New York, 1985; Vol. 33, p 275.
(11) Geiger, W. E. *Acc. Chem. Res.* **1995**, *28*, 351.
(12) Bard, A. J.; Faulkner, L. R. *Electrochemical Methods*; John Wiley and Sons: New York, 1980.
(13) Pierce, D. T.; Geiger, W. E. *J. Am. Chem. Soc.* **1992**, *114*, 6063.
(14) (a) Ascenso, J. R.; Azevedo, C. G.; Gonçalves, I. S.; Herdtweck, E.; Moreno, D. S.; Pessanha, M.; Romão, C. C. *Organometallics* **1995**, *14*, 3901. (b) Ascenso, J. R.; Azevedo, C. G.; Gonçalves, I. S.; Herdtweck, E.; Moreno, D. S.; Romão, C. C.; Zühlke, J. *Organometallics* **1994**, *13*, 429. (c) Gonçalves, I. S.; Romão, C. C. *J. Organomet. Chem.* **1995**, *486*, 155. (d) Gonçalves, I. S.; Herdtweck, E.; Romão, C. C.; Royo, B. *J. Organomet. Chem.* **1999**, *580*, 169. (e) Calhorda, M. J.; Gamelas, C, A.; Romão, C. C.; Veiros, L. F. *Eur. J. Inorg. Chem.* **2000**, *331*. (f) Gamelas, C. A. Ph.D. Dissertation, Instituto de Tecnologia Quimíca e Biológica, Oeiras, Portugal, 2000.
(15) Gamelas, C. A.; Herdtweck, E.; Lopes, J. P.; Romão, C. C. *Organometallics* **1999**, *18*, 506.

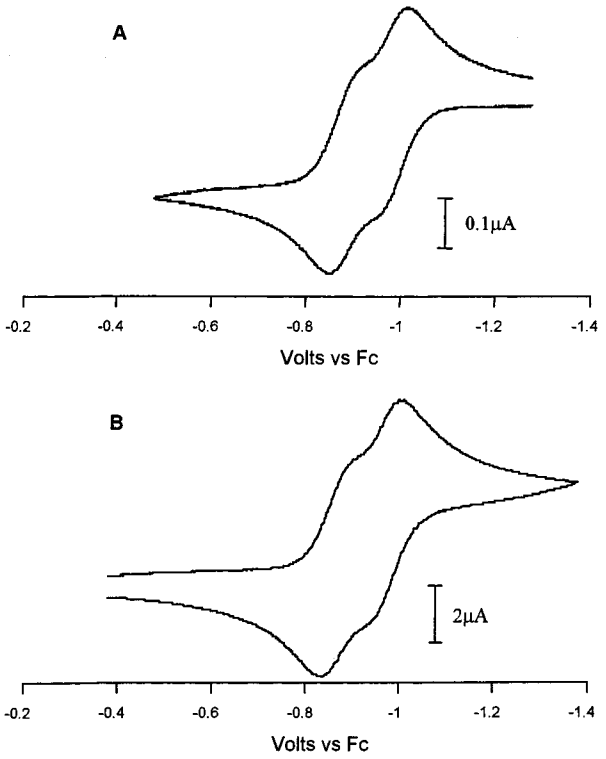

Figure 1. Cyclic voltammograms of **1** (top, A) and $\mathbf{1}^{2+}$ (bottom, B) in CH_3CN/0.1 M $[NBu_4][PF_6]$ at 298 K, scan rate 0.1 V/s. (A) 0.45 mM **1** at a 0.5 mm Pt disk. (B) 0.59 mM $\mathbf{1}^{2+}$ at a 2 mm Pt disk.

oxidation, leading to 18-electron metal configurations for both even-electron species.

In the case of bis(phosphite) complexes **1** and $\mathbf{1}^{2+}$, the one-electron intermediate $\mathbf{1}^{+}$ was quite stable in solution (vide infra), but attempts to obtain pure crystals from the comproportionation reaction mixture of **1** and several salts of $\mathbf{1}^{2+}$ (BF_4^-, PF_6^-, BPh_4^-) were unsuccessful. Complexes which were partially deuterated at the indenyl ring were obtained for both **1** and $\mathbf{1}^{2+}$ by procedures described in the Experimental Section and Supporting Information.

Reaction of $[(\eta^5\text{-Ind})(Cp)Mo(NCMe)_2]^{2+}$ with excess KCN in CH_2Cl_2/NMF gives the cyanide complex, $(\eta^5\text{-Ind})(Cp)Mo(CN)_2$. To the best of our knowledge, this is the third example of a cyano derivative of Mo and W metallocenes, with the other ones being $Cp_2W(OR)CN$[16a] and $Cp_2Mo(CN)_2$.[16b]

Electrochemical Studies. The four complexes studied ($\mathbf{1}^{2+}$, **1**, $\mathbf{2}^{2+}$, and **3**) all exhibited two closely spaced, diffusion-controlled cyclic voltammetry (CV) waves at Pt, Au, and glassy carbon disk electrodes in either CH_2Cl_2 or CH_3CN containing $[NBu_4][PF_6]$ as the supporting electrolyte. No electrode history or adsorption problems were encountered. Except at high scan rates, all the CV waves obeyed the diagnostics of Nernstian one-electron processes with stable reaction products. Thus, each electron transfer is chemically reversible with relatively high heterogeneous charge-transfer rates (k_s values). As will be shown below, the k_s value of the Mo(IV)/Mo(III) process is in each case slightly lower than that of the Mo(III)/Mo(II) process for the same compound.

Complexes $\mathbf{1}^{2+}$ and **1** showed the expected similarities in two reversible reduction waves for the former and two reversible oxidation waves for the latter (Figure 1). CV scans of neutral **1** in CH_3CN demonstrated two closely spaced oxidations with $E_{1/2}$ values of −0.950 V [$E_{1/2}(2)$] and −0.837 V [$E_{1/2}(1)$] versus Fc (Eq 2, Table 1). The limited potential difference of these two

$$\mathbf{1}^{2+} \overset{E_{1/2}(1)}{\rightleftharpoons} \mathbf{1}^{+} \overset{E_{1/2}(2)}{\rightleftharpoons} \mathbf{1} \qquad (2)$$

waves [$\Delta E_{1/2} = E_{1/2}(1) - E_{1/2}(2) = 113$ mV] required the use of digital simulations to obtain precise $E_{1/2}$ values (Figure 2). When the scan rate (υ) was increased above about 10 V/s, the peak separations of the couple for $\mathbf{1}^{+}/\mathbf{1}^{2+}$ [$E_{1/2}(1)$, −0.837 V] increased compared to those for the $\mathbf{1}/\mathbf{1}^{+}$ couple [$E_{1/2}$ (2), −0.950 V]. Agreement of the experimental CVs with digital simulations from 0.1 V/s < υ < 80 V/s established heterogeneous electron-transfer parameters: $k_s(1) = 0.4$ cm/s, $\alpha(1) = 0.58$, $k_s(2) = 1$ cm/s, and $\alpha(2) = 0.5$ (Table 1).

Square-wave voltammetry (SWV) was also helpful in characterizing the redox properties of **1** and $\mathbf{1}^{2+}$. The response of **1** over the frequency range 5−1500 Hz in CH_3CN was as

Table 1. $E_{1/2}$ Values (Volts vs Ferrocene) and Heterogeneous Electron Transfer Rates (k_s, in cm s^{-1}) for Indenyl-Molybdenum Complexes Measured by Cyclic Voltammetery at Glassy Carbon Electrode, 0.1 M $[NBu_4][PF_6]$ Electrolyte

compound	solvent	$E_{1/2}(1)$[a]	$E_{1/2}(2)$[b]	$\Delta E_{1/2}$[c]	$k_s(1)$	$k_s(2)$
1	CH_2Cl_2	−0.785	−1.004	0.219		
1	CH_3CN	−0.837	−0.950	0.113	0.40[d]	1.0
$\mathbf{1}[BF_4]_2$	CH_2Cl_2	−0.792	−1.002	0.210		
$\mathbf{2}[BF_4]_2$	CH_2Cl_2	−0.709	−0.914	0.205		
$\mathbf{2}[BF_4]_2$	CH_3CN	−0.716	−0.877	0.161		
3	CH_2Cl_2	−1.578	−1.914	0.336		
3	CH_3CN	−1.531	−1.787	0.256	0.03	0.06

[a] Mo(IV)/Mo(III) couple. [b] Mo(III)/Mo(II) couple. [c] $\Delta E_{1/2} = E_{1/2}(1) - E_{1/2}(2)$. [d] A value of 0.05 cm s^{-1} was observed for $k_s(1)$ in square wave voltammetry experiments.

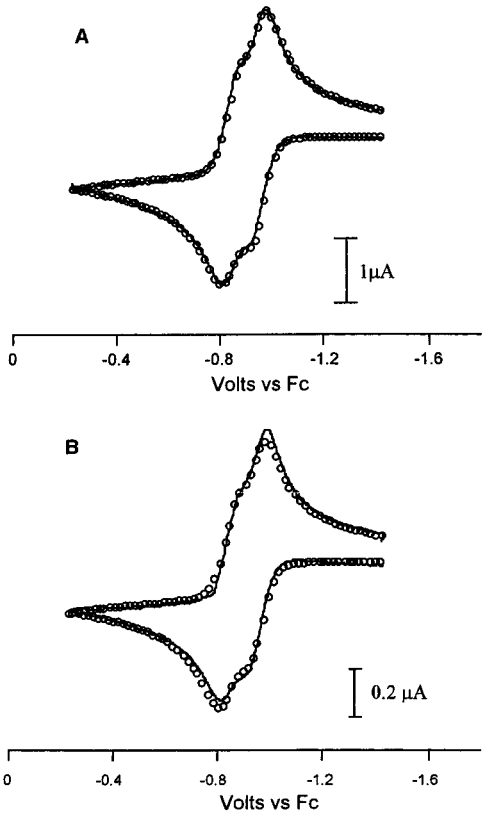

Figure 2. Comparison of experimental (solid lines) and simulated (open circles) CV curves for **1** at two different scan rates. Experimental data taken on 0.50 mM **1** in CH_3CN at (A) 10 V/s, 0.5 mm Pt disk, and (B) 80 V/s, 0.125 mm Pt disk. Simulation parameters in text.

(16) (a) Green, M. L. H.; Lindsell, W. E. *J. Chem. Soc. A* **1969**, 2150. (b) Martins, A. M. Ph.D. Dissertation, Universidade Técnica de Lisboa, Portugal, 1991.

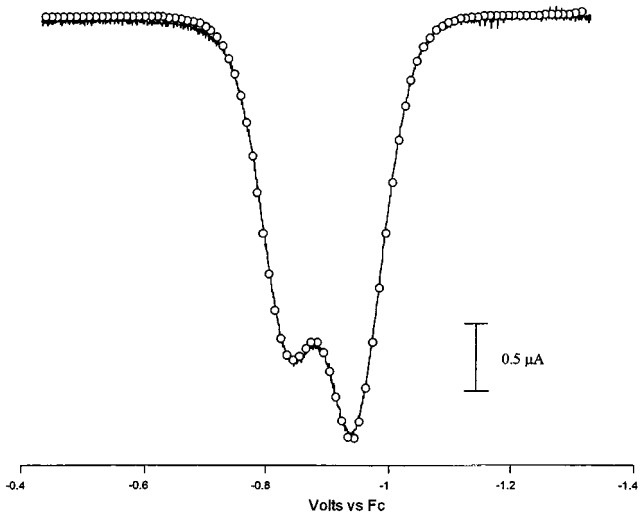

Figure 3. Comparison of experimental (solid) and simulated (circles) square wave (SW) voltammograms of 0.5 mM **1** in CH_3CN at 298 K using a 0.5 mm Pt disk at 600 Hz SW frequency.

expected[17] for a complex undergoing two relatively rapid one-electron transfers. The diminished peak height observed for the $\mathbf{1}^+/\mathbf{1}^{2+}$ wave at high frequencies (Figure 3) is indicative of a slower heterogeneous electron transfer for this couple compared to $\mathbf{1}/\mathbf{1}^+$. Simulations of the square-wave responses at various frequencies are largely consistent with the parameters measured by cyclic voltammetry and given in Table 1.

The largest discrepancy was in the value determined for the heterogeneous charge-transfer rate of the $\mathbf{1}^+/\mathbf{1}^{2+}$ couple, where $k_s(1)$ was found to be 0.05 cm s^{-1}, somewhat lower than the value of 0.4 cm s^{-1} determined by cyclic voltammetry. The quantitative difference between these values does not alter the conclusion that the rate of heterogeneous electron transfer for *oxidation* of the radical $\mathbf{1}^+$ to $\mathbf{1}^{2+}$ is less than that of the *reduction* of the same radical to **1** ($\sim$1 cm s^{-1} by both methods). However, the rate constants for either oxidation or reduction of $\mathbf{1}^+$ are sufficiently large that the inner-sphere reorganizational barriers of both couples must be relatively small.[18]

The oxidation of **1** in dichloromethane also followed an EE mechanism, confirmed by digital simulations up to scan rates of 2 V/s. After resistance corrections, the waves are essentially Nernstian, but k_s values were not precisely determined owing to the quantitative uncertainties typical for fast electron transfers in low-polarity solvents. The two oxidations have a larger potential difference ($\Delta E_{1/2} = 219$ mV) than that found in CH_3CN (113 mV, Table 1), reflecting an increased disproportionation energy for $\mathbf{1}^+$ in CH_2Cl_2. For this reason, dichloromethane was the solvent of choice for generating the one-electron intermediate $\mathbf{1}^+$ (and $\mathbf{2}^+$ as well) for ESR studies.

Bulk electrolysis experiments were performed in either CH_3CN or CH_2Cl_2 solutions. When a yellow solution of **1** is oxidized in CH_3CN at $E_{appl} = -0.65$ V, $\mathbf{1}^{2+}$ is produced with release of 1.9 F/equiv. Reverse (reductive) electrolysis of this orange solution at $E_{appl} = -1.1$ V regenerated **1** (1.9 F/equiv) without loss. When **1** was electrolyzed in CH_2Cl_2, an applied potential (-0.87 V) that is intermediate between the two $E_{1/2}$ values was used in order to favor formation of the monocation, $\mathbf{1}^+$. With passage of 0.91 F/equiv, a sample of the very dark orange solution of $\mathbf{1}^+$ was taken for ESR measurements, after which changing E_{appl} to -1.2 V resulted in the quantitative regeneration of **1**.

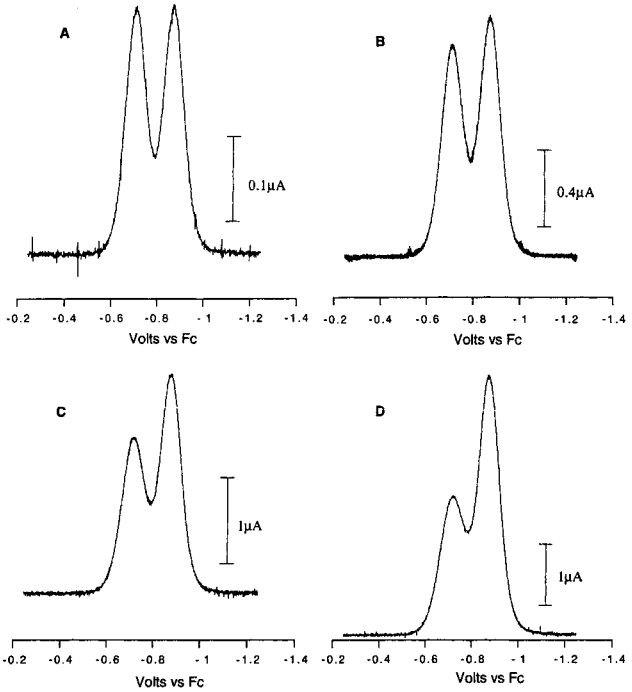

Figure 4. Square wave voltammograms of 0.64 mM $\mathbf{2}^{2+}$ in CH_3CN at a 0.5 mm Pt disk electrode, $T = 298$ K. SW scan rates were (A) 5 Hz, (B) 100 Hz, (C) 400 Hz, and (D) 1000 Hz.

Reduction of the dppe complex, $\mathbf{2}^{2+}$, also proceeds in two reversible one-electron processes in either CH_3CN or CH_2Cl_2. Although the potentials of $\mathbf{2}^{2+}$ are slightly positive of those observed for $\mathbf{1}^{2+}$, the voltammetric characteristics of these two dications, including chemical reversibility, electron-transfer rates, and $\Delta E_{1/2}$ values, are otherwise quite similar (Table 1). At higher CV scan rates, the Mo(IV)/Mo(III) couple at $E_{1/2}(1) = -0.71$ V became obviously quasireversible, whereas the second reduction at $E_{1/2}(2)$ retained the characteristics of a more rapid charge-transfer reaction [e.g., in acetonitrile at $\nu = 5$ V s^{-1}, $\Delta E_p(1) = 94$ mV, and $\Delta E_p(2) = 70$ mV]. In square-wave voltammograms, the first cathodic wave at -0.71 V diminished in height compared to the second at higher frequencies (Figure 4). The resulting conclusion that the electron-transfer rate of $\mathbf{2}^{2+}/\mathbf{2}^+$ is lower than that of $\mathbf{2}^+/\mathbf{2}$ is similar to the results detailed above for complex **1** and its ions. Bulk coulometry at the potential of the first reduction of $\mathbf{2}^{2+}$ in CH_2Cl_2 ($E_{appl} = -0.8$ V) showed that the radical intermediate, $\mathbf{2}^+$, is persistent. An initially pink solution of the dication $\mathbf{2}^{2+}$ became brown with passage of 0.95 F/equiv, and a sample was taken for ESR analysis of $\mathbf{2}^+$. Continuation of the electrolysis at a more negative potential ($E_{appl} = -1.1$ V) consumed one more electron per mole and gave the bright orange color of neutral **2**. Back-electrolysis at -0.5 V regenerated $\mathbf{2}^{2+}$ in about 90% yield.

Electrochemical studies were also performed on **3**, a biscyanide compound which is neutral as the Mo(IV) complex, thereby distinguishing it from the analogous dications $\mathbf{1}^{2+}$ and $\mathbf{2}^{2+}$. The neutral complex undergoes two successive one-electron reductions (Eq 3) as the η^5-indenyl complex **3** goes to a dianion, $\mathbf{3}^{2-}$, which is assumed to have an η^3-bonded indenyl ligand.[19] The

$$\mathbf{3} \overset{E_{1/2}(1)}{\rightleftharpoons} \mathbf{3}^- \overset{E_{1/2}(2)}{\rightleftharpoons} \mathbf{3}^{2-} \qquad (3)$$

(17) Osteryoung, J.; O'Dea, J. J. In *Electroanalytical Chemistry*; Bard, A. J., Ed.; Marcel Dekker: New York, 1986, vol 14, pp 209 ff.

(18) This statement draws on the original Marcus theory (e.g., see: Marcus, R. A. *J. Chem. Phys.* **1965**, *43*, 679.). Some leading references to k_s values for organometallic complexes: Weaver, M. J.; Gennett, T. *Chem. Phys. Lett.* **1985**, *113*, 213. Chin, T. T.; Geiger, W. E.; Rheingold, A. L. *J. Am. Chem. Soc.* **1996**, *118*, 5002.

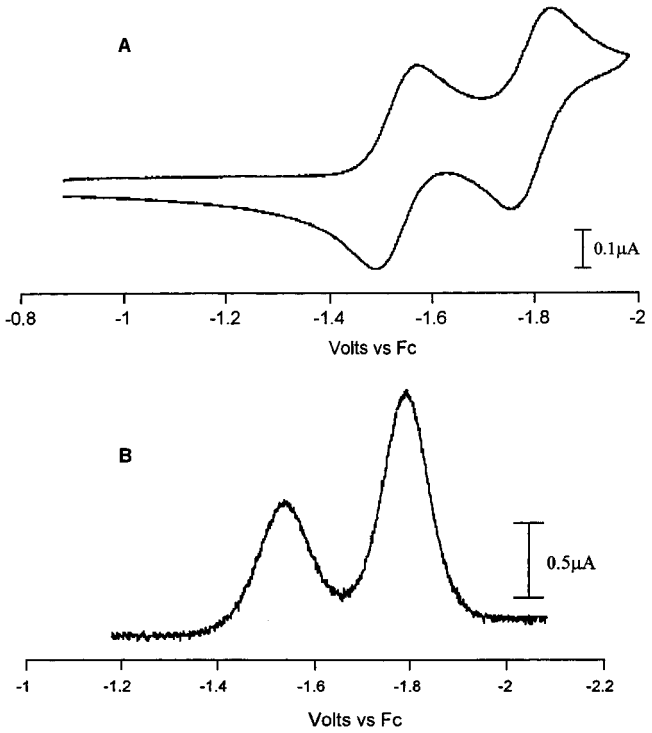

Figure 5. Cyclic voltammetry (A, top) and square wave voltammetry (B, bottom) scans of 0.61 mM **3** in CH_3CN at 298 K. CV at 0.5 mm Pt disk, scan rate 0.2 V/s; SWV at 0.5 mm Pt disk, 700 Hz.

potentials of the two waves (−1.53 and −1.79 V in acetonitrile) are considerably negative of those observed for the same changes in formal electron counts for complexes **1** and **2** and are also more highly separated than those observed for the bisphosphite or -phosphine complexes (Table 1). CV scans of **3** in CH_3CN once again showed that the electron-transfer rate of the Mo(IV)/Mo(III) couple at $E_{1/2}(1)$ was lower than that of the Mo(III)/Mo(II) couple at $E_{1/2}(2)$, with estimates[20] of $k_s(1) = 0.03$ cm/s and $k_s(2) = 0.06$ cm/s being obtained from ΔE_p values over the range $\upsilon = 0.2-5$ V/s at a 500 μm Pt disk. Representative CV and SWV scans are shown in Figure 5.

Bulk electrolysis of a red solution of **3** in CH_2Cl_2 at a potential negative of $E_{1/2}(1)$ passed 0.94 F/equiv and produced a red-brown solution of monoanion $\mathbf{3}^-$, the charge of which was confirmed by steady-state voltammograms. This solution was sampled for ESR analysis. Reoxidation of the solution at $E_{appl} = -1.1$ V regenerated **3** in high yield. An attempt to produce dianion $\mathbf{3}^{2-}$ failed, as the Mo(II) product appears to undergo slow regeneration to $\mathbf{3}^-$ in this solvent.

ESR Measurements. ESR spectra of isoelectronic radicals $\mathbf{1}^+$, $\mathbf{2}^+$, and $\mathbf{3}^-$ were obtained on both frozen and fluid solutions generated by coulometric oxidation or reduction of the appropriate precursor. In the case of $\mathbf{1}^+$, the radical was also generated by the comproportionation reaction of equimolar quantities of **1** and $\mathbf{1}^{2+}$, giving spectra identical to those of electrochemically generated samples. The frozen spectra were sufficiently broad and poorly resolved (Supporting Information Figure S1) that an interpretation was not attempted. In contrast, fluid solution spectra displayed line widths of 3−5 G and were

(19) Neutral **3** also gives a one-electron oxidation wave with $E_{1/2} = 0.67$ V versus Fc which is chemically irreversible at scan rates below 0.2 V/s. The wave has some reversibility at higher scan rates, an i_{rev}/i_{fwd} value of 0.83 being obtained for a CV scan rate of 3 V/s.

(20) These k_s values are taken from the results of a single CV experiment in which IR compensation was not employed. They should be taken as lower limits. The apparent k_s value of ferrocene was about 0.1 cm/s under these conditions.

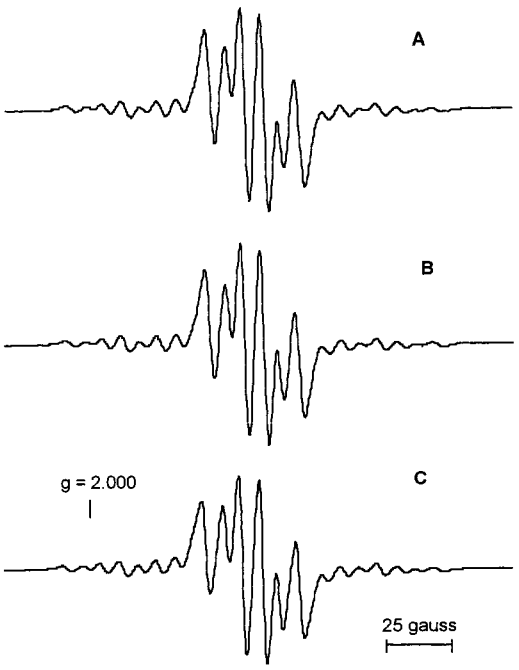

Figure 6. Fluid solution ESR spectra in CH_2Cl_2 at ambient temperature of (A) electrochemically generated $\mathbf{1}^+$; (B) partially deuterated $\mathbf{1}^+$ under same conditions; (C) simulated spectrum using $g_{iso} = 1.963$, a(Mo) = 21.75 G, a(P) = 14.50 G, and a(H) = 8.00 G. Line width = 3.5 G.

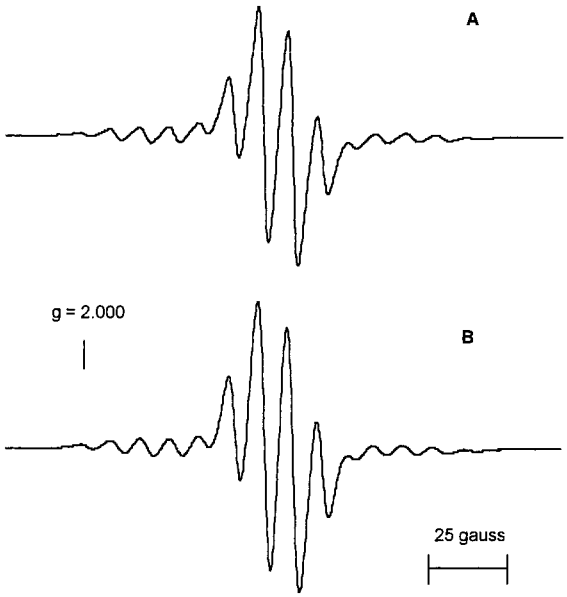

Figure 7. Comparison of simulated (A, top) and experimental (B, bottom) ESR spectra of $\mathbf{2}^+$ generated through ambient-temperature oxidation of **2** by ferrocenium ion in CH_2Cl_2. Simulated values: $g_{iso} = 1.965$, a(Mo) = 19.00 G, a(P) = 9.50 G, and a(H) = 9.50 G. Line width = 3.5 G.

readily interpreted and simulated (Figures 6 and 7). All three radicals display hyperfine splittings from Mo ($\langle a \rangle_{Mo} = (17.3-21.4) \times 10^{-4}$ cm^{-1}, $I = 5/2$ for ^{95}Mo and ^{97}Mo, combined 25% natural abundance) and either one (in the case of $\mathbf{3}^-$) or three (for $\mathbf{1}^+$ or $\mathbf{2}^+$) 100% abundant, spin-1/2 nuclei. Two of the ligand splittings in $\mathbf{1}^+$ and $\mathbf{2}^+$ are assigned to ^{31}P (13.3×10^{-4} cm^{-1} for $\mathbf{1}^+$ and 8.7×10^{-4} cm^{-1} for $\mathbf{2}^+$, Table 2) on the basis of their absence in the spectrum of $\mathbf{3}^-$, a complex which lacks phosphorus nuclei. The third ligand splitting in $\mathbf{1}^+$ and $\mathbf{2}^+$, as well as the single ligand splitting in $\mathbf{3}^-$, is assigned as a_H, with values of $(6.4-8.7) \times 10^{-4}$cm^{-1}.

Table 2. Selected Isotropic ESR Parameters for Formal Mo(III) Complexes in CH_2Cl_2; Hyperfine Splittings in Units of 10^{-4} Reciprocal Centimeters (e.g., $\langle a \rangle_{Mo} = 20 \times 10^{-4}$ cm^{-1})[a]

radical	$\langle g \rangle$	$\langle a \rangle_{Mo}$	$\langle a \rangle_{P}$	$\langle a \rangle_{H}$	T (K)
$\mathbf{1}^+$	1.9628	20.0	13.3	7.4	298
d-$\mathbf{1}^+$	1.9628	20.0	13.3	7.4	298
$\mathbf{2}^+$	1.9650	17.5	8.7	8.7	298
$\mathbf{3}^-$	1.9600	22.1	*a*	6.4	250

[a] No phosphorus atoms in this molecule.

Table 3. Selected Bond Distances (Å) and Angles (deg) in the Molybdenum Coordination Sphere of Complexes **1**and $\mathbf{1}^{2+}$

Bond Distance

	1	$\mathbf{1}^{2+}$
Mo−C(31)	2.327(6)	2.318(6)
Mo−C(32)	2.357(6)	2.299(6)
Mo−C(33)	2.359(6)	2.318(6)
Mo−C(34)	2.310(6)	2.327(7)
Mo−C(35)	2.291(6)	2.356(6)
Mo−C(2)	2.209(6)	2.277(7)
Mo−C(3)	2.362(6)	2.313(6)
Mo−C(4)	(3.039(6))	2.429(5)
Mo−C(5)	(3.029(6))	2.452(5)
Mo−C(6)	2.359(6)	2.290(6)
Mo−P(1)	2.404(3)	2.468(3)
Mo−P(2)	2.377(2)	2.462(3)
Mo−Cp	1.998	1.999
Mo−Ind	2.069	2.014

Bond Angle

	1	$\mathbf{1}^{2+}$
P(1)−Mo-P(2)	88.51(8)	86.72(8)
Cp−Mo−Ind	123.6	135.5
Cp−Mo−P(1)	113.7	106.7
Cp−Mo−P(2)	117.0	104.7
Ind−Mo−P(1)	105.8	105.9
Ind−Mo−P(2)	102.2	106.7

[a] Ind refers to the indenyl ligand and represents the centroid of five members for complex **1** and the midpoint of the two carbon atoms adjacent to the six membered ring (atoms C(42) and C(49), see Figure 8a) for $\mathbf{1}^{2+}$. Cp denotes the centroid of cyclopentadienyl ring for both complexes.

To further clarify the assignment of the *proton* hyperfine splitting in these radicals, a sample of $\mathbf{1}^+$ which was 70% deuterated in the indenyl 1,3-positions was prepared. The radical was generated again by electroreduction of a sample of the corresponding partially deuterated dication $\mathbf{1}^{2+}$ in dichloromethane. The resulting spectrum was identical to that of the protio sample (Figure 6), eliminating the possibility that either of the protons on the C(1) or C(3) indenyl carbons is responsible for a_H. The most credible source of this hyperfine splitting is therefore the proton on the indenyl C(2) carbon (see drawing).

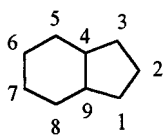

This assignment for $\mathbf{1}^+$, and the analogous ones intimated for $\mathbf{2}^+$ and $\mathbf{3}^-$, are not accounted for by the McConnell relationship ($a_H = -Q\rho^{\pi}_C$),[21] which would require a spin density of ~30% at C(2). The comparatively large hyperfine splitting (hfs) from H(2) is better addressed by the recent work of Braden and Tyler,[22] who showed that ligand hyperfine splittings of organometallic radicals are often greatly affected by distributions in orbitals other than the singly occupied molecular orbital (SOMO). It will be shown below that the abnormally large values of $a_{H(2)}$ are well accounted for in DFT calculations.

(21) ρ^{π}_C is the p−π spin density on the carbon atom; Q varies with the charge and size of the overall π-ligand but is generally in the range 23−30 × 10^{-4} cm^{-1}. See: Carrington, A.; McLachlan, A. D. *Introduction to Magnetic Resonance*; Harper and Row: New York, 1967; p. 83. Weil, J. A.; Bolton, J. R.; Wertz, J. E. *Electron Paramagnetic Resonance*; Wiley-Interscience: New York, 1994; p 243.

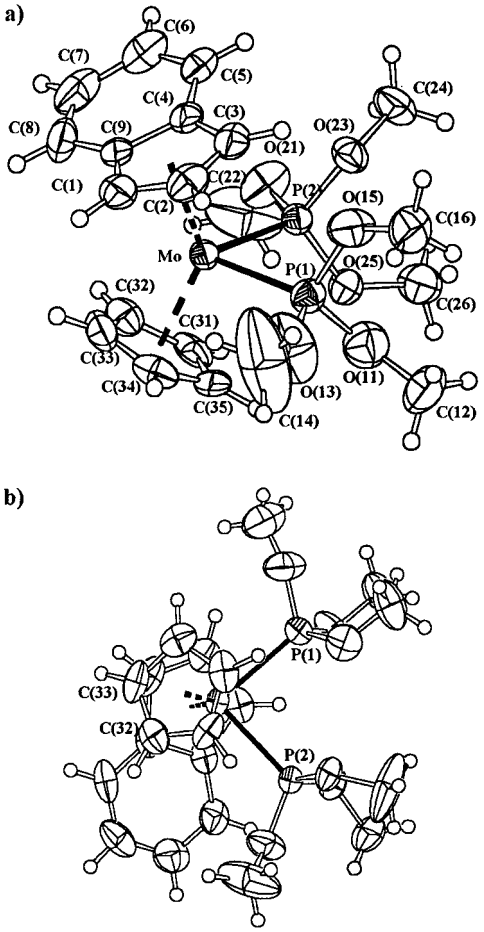

Figure 8. Molecular structure of the complex cation [(η^5-Ind)(Cp)-Mo{P(OMe)$_3$}$_2$]$^{2+}$ ($\mathbf{1}^{2+}$) with ellipsoids drawn at 40% probability: (a) view parallel to the plane P−Mo−P with labeling scheme adopted and (b) view perpendicular to the P−Mo−P plane.

Crystallography. The crystal structures of complexes [(η^5-Ind)(Cp)Mo{P(OMe)$_3$}$_2$][BF_4]$_2$ ([$\mathbf{1}^{2+}$][BF_4]$_2$) and (η^3-Ind)(Cp)-Mo(P(OMe)$_3$)$_2$ (**1**) were determined using single-crystal X-ray diffraction. The asymmetric unit consists of one cation and two anions for complex [$\mathbf{1}^{2+}$][BF_4]$_2$ and a discrete molecule for complex **1.** The dication $\mathbf{1}^{2+}$ is shown in Figure 8, and complex **1** is shown in Figure 9, in two different views, side and top. Selected bond angles and distances are listed in Table 3 for both compounds. In the cation, $\mathbf{1}^{2+}$, the five Mo−C distances, ranging from 2.276(7) to 2.453(5) Å, indicate that the indenyl ligand is η^5 coordinated to the metal. In complex **1**, only three Mo−C distances are within bonding distance, with the indenyl ligand being linked to the metal center by carbon atoms C(2) [2.209(6) Å], C(3) [2.362(6) Å], and C(1) [2.359(6) Å], Table 3. The other two carbon atoms of the C5 ring, C(4) and C(9), are not bonded to the metal atom (distances of 3.039(6) and 3.029(6) Å, respectively), leading to an η^3 coordination of the indenyl ligand. Two P(OMe)$_3$ ligands and one η^5-cyclopentadienyl ring complete the molybdenum coordination sphere of

(22) (a) Braden, D. A.; Tyler, D. R. *J. Am. Chem. Soc.* **1998**, *120*, 942. (b) Braden, D. A.; Tyler, D. R. *Organometallics* **2000**, *19*, 1175.

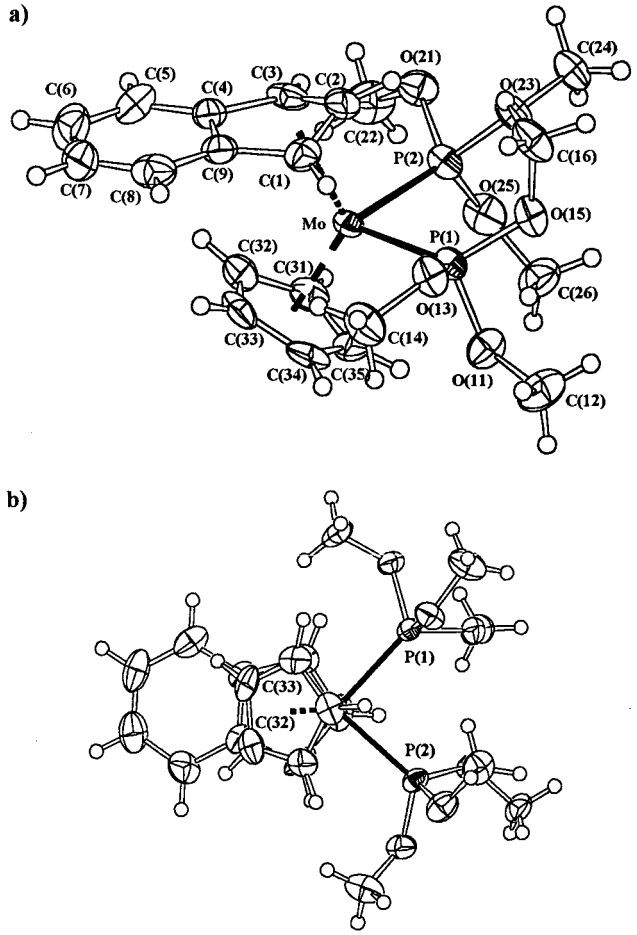

Figure 9. Molecular structure of complex (η^3-Ind)(Cp)Mo{P(OMe)$_3$}$_2$ (**1**) with ellipsoids drawn at 40% probability: (a) view parallel to the P−Mo−P plane with labeling scheme adopted and (b) view perpendicular to the P−Mo−P plane.

both complexes. The values of the subtended angles (including the centroids of the π label moieties) at the molybdenum center show a distorted pseudotetrahedral arrangement for complexes in both oxidation states.

The average Mo−P distance in $\mathbf{1}^{2+}$ [2.465(3) Å] is significantly longer than in complex **1** [2.390(2) Å], owing to the lower formal Mo oxidation state in the latter. The angle P−Mo−P in $\mathbf{1}^{2+}$ [86.72(8)°] is slightly smaller than in **1** [88.51(8)°], but both values fall within the range observed for related derivatives.[23]

To compare X-ray structures of the present complexes with other [(Ind)(Cp)MLL′]$^{n+}$ systems, a search on the Cambridge Structural Data Base (CSD) was undertaken.[23] Only three complexes were obtained, and these are listed in Table 4 together with their REFCODES, sources, and relevant structural parameters used in the characterization of the η^3 and η^5 indenyl complexes, as well as the structural data for one molybdenum complex not yet available in the CSD. Several parameters were introduced by Faller et al.[24] to characterize the coordination of the indenyl ligands to a metal center. Among them, the folding Ω angle, defined here as the angle between the plane formed by C(3), C(4), C(9), C(1) and that formed by C(3), C(2), and C(1), shows the most straightforward relationship with indenyl hapticity. The ligand is almost planar when η^5 coordination occurs, and so, the angle is very small. Thus, in the cation, $\mathbf{1}^{2+}$, the indenyl ligand shows a small Ω angle of 4.1°, comparable to those found for the other transition metal complexes quoted in Table 4 containing a single η^5 indenyl ligand.

In contrast, the indenyl ring in complex **1** displays a pronounced folding, characteristic of η^3 coordination, across the vector C(1)−C(3), leading to a Ω angle of 21.7°. In fact, this value is only 0.4° larger than that found for complex **D**, which also contains an η^3-indenyl ring. The indenyl rotation angle, λ, is easily defined for [(η^5-Ind)$_2$MLL′]$^{n+}$ systems as the angle between the projections of the two vectors determined by the centroids of the five and six member rings on the plane L−M−L′. For the metal systems containing η^5-Cp and η^3-Ind rings, this definition of λ must necessarily be adjusted. For the Cp ring, the centroid of the six-membered ring is replaced by the midpoint of the two carbon atoms trans to the L and L′ ligands [atoms C(32) and C(33) in complexes $\mathbf{1}^{2+}$ and **1**, (see Figures 8 and 9)]. For η^3-indenyl rings, the centroid of the five membered ring is replaced by the midpoint of the two carbon atoms adjacent to the six-membered ring [atoms C(1) and C(3) in complex **1** (see Figure 9)]. For a fully eclipsed arrangement of the two π-ligands, a λ angle of 0° is expected, while a fully staggered arrangement will correspond to a λ angle of 180°. The λ value for complex $\mathbf{1}^{2+}$ is 117.1°, indicating a partially staggered arrangement of the indenyl and Cp rings, while in complex **1** these rings are almost eclipsed, with a λ angle of 7.1°. The λ value in the η^3-indenyl complex is 0.0°, while, in all the related complexes, λ varies from 93.5° to 110.5° (Table 4). These preferred values are most likely caused by steric intramolecular effects, as is discussed in a following section.

Theoretical Studies: Bonding and Structures. Here, we address electronic and structural aspects of **1** and $\mathbf{1}^{2+}$ using extended Hückel (EH) and DFT calculations. The ultimate goal of the DFT calculations was to determine the accuracy of this method in probing the structure of odd-electron $\mathbf{1}^{+}$. Hence, the DFT structural predictions on **1** and $\mathbf{1}^{2+}$ were compared with the geometries established by X-ray results before proceeding to use the method to predict the structure of $\mathbf{1}^{+}$. These efforts were aided by consideration of the calculationally easier dicarbonyl complexes, [(η^5-Ind)CpMo(CO)$_2$]$^{2+}$ and (η^3-Ind)-CpMo(CO)$_2$; the X-ray structure of the neutral dicarbonyl complex was reported earlier.[14a]

Taking into account that an η^5-indenyl group is a three-electron-pair donor, the interaction diagram, based on EH calculations, between this anionic ligand and the CpMo(CO)$_2^+$ fragment (Figure 10, left side) shows that these electrons are donated to three empty metal orbitals, 2a′, 1a″, and 3a′, and that only bonding orbitals are occupied. In the schematic diagram, only the strongest interactions are drawn, although there is mixing as a result of low symmetry. If another pair of electrons is added, as when reduction takes place, it will occupy the high energy Mo−indenyl antibonding orbital 4a′, which is clearly a very unfavorable electronic situation. When the ligand becomes η^3, these electrons occupy the equivalent 4a′ orbital (right side of Figure 10), which is still antibonding, but much less so. Indeed, only three carbon atoms from the indenyl group contribute to this orbital; the carbon atoms in the junction move away from the metal, therefore relieving the antibonding interaction. For the sake of simplicity, the indenyl ligand in the η^5-Ind compound is rotated from its position in the crystal structure to achieve C_s symmetry. Qualitatively, it makes little difference. This side of the diagram can be viewed in a different way. As the metal is reduced and takes up two more electrons, the indenyl ligand formally donates only two pairs of electrons,

(23) Allen, F. H.; Davies, J. E.; Galloy, J. J.; Johnson, O.; Kennard, O.; Macrae, C. F.; Mitchell, E. M.; Mitchel, G. F.; Smith, J. M.; Watson, D. G. *J. Chem. Inf. Comput. Sci.* **1991**, *31*, 187.

(24) Faller, J. W.; Crabtree, R. H.; Habib, A. *Organometallics* **1985**, *4*, 929.

Table 4. Compounds, REFCODES, Sources, and Structural Parameters (deg) Relevant in the Characterization of the η^3- and η^5-Indenyl Complexes

complex	REFCODE	complex	λ	Ω_{Ind}; Ω_{Cp}	ref
$\mathbf{1}^{2+}$		$[(\eta^5\text{-Ind})(\eta^5\text{-Cp})Mo(P(OCH_3)_3)_2]^{2+}$	117.1	4.1; 0.6	*b*
1		$(\eta^3\text{-Ind})(\eta^5\text{-Cp})Mo(P(OCH_3)_3)_2$	7.1	21.7; 0.2	*b*
A		$(\eta^5\text{-Ind})(\eta^5\text{-Cp})Mo(CN)_2$[a]	110.5	4.5; 1.4	14f
			99.3	3.9; 1.0	
B	LEHXEB	$[(\eta^5\text{-Ind})(\eta^5\text{-Cp})Mo(CO)(NCCH_3)]^{2+}$	93.5	5.0; 0.7	14a
C	SIMDOH, SIMDOH10	$(\eta^5\text{-Ind})(\eta^5\text{-Cp})Ta((CH_2)_2Ir(CO)_2)$	102.3	5.5; 0.3	55
D	ZEGTUA	$(\eta^3\text{-Ind})(\eta^5\text{-Cp})Mo(CO)_2$	0.0	21.3; 2.1	14a

[a] Two molecules in the unit cell. [b] This work.

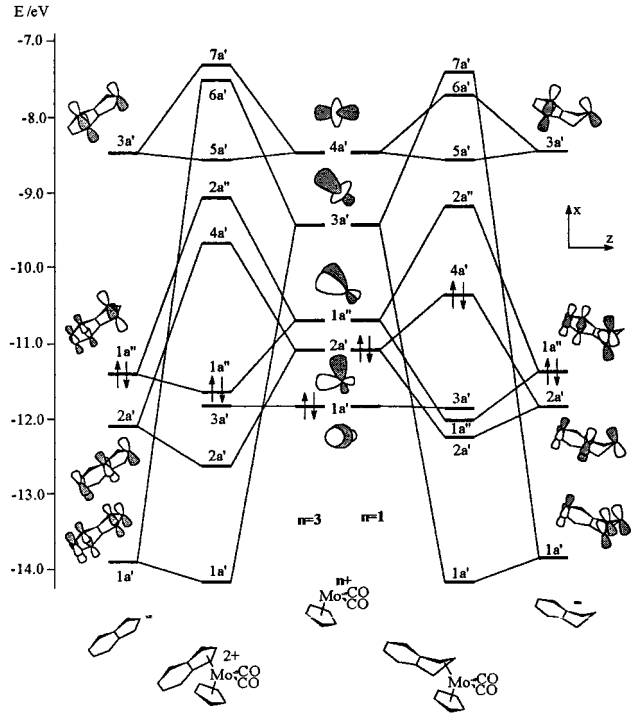

Figure 10. Interaction diagram between the $[CpMo(CO)_2]^{2+}$ fragment and η^5-Ind (left, $n = 3$) or η^3-Ind (right, $n = 1$); the two arrows designate the HOMO.

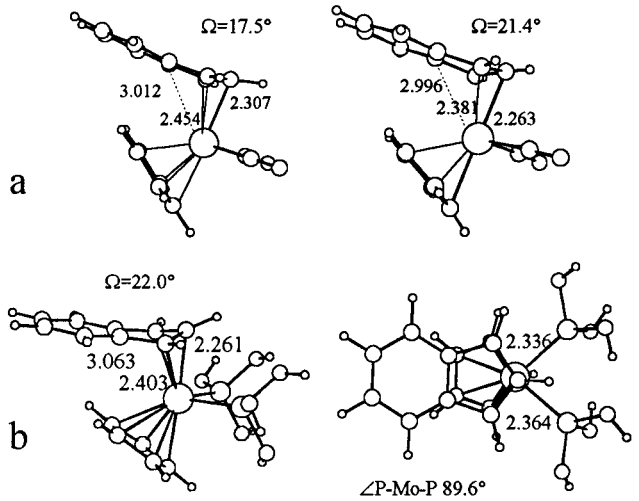

Figure 11. Structure of $(\eta^3\text{-Ind})CpMo(L)_2$ complexes. (a) L = CO, calculated (DFT, left) and experimental (right). (b) L = $P(OH)_3$, calculated (DFT), side view (left) and top view (right).

forming two metal−indenyl bonds. The third possible bond has both the bonding and antibonding orbitals occupied and therefore does not contribute to the bonding. The conclusion that *reductively induced bending of the indenyl ligand relieves antibonding character in the new HOMO* is very similar to what happens when the indenyl slippage is induced by the addition of ligands.[25]

The geometry of the radical intermediate, $[(Ind)CpMoL_2]^+$, was investigated by DFT calculations. To check the reliability of the calculated structures, results on the neutral and dicationic complexes were first optimized against those of the known systems, putting emphasis on the metal−carbon distances to the indenyl five-membered ring and the folding (Ω) of the indenyl ligand.

The DFT calculations (see Experimental Section for further details) were performed at the nonlocal level, but only the position of the indenyl group and the angles between ligands were optimized for the carbonyl complexes. For the neutral $(\eta^3\text{-Ind})(Cp)MoL_2$ complexes, the three known structures for L = CO, $P(OMe)_3$, and dppe all have approximate C_s symmetry, with the two rings being almost eclipsed. Therefore, the optimization for our model dicarbonyl compound was carried out with imposed C_s symmetry. In Figure 11a, we show the most important structural parameters for the optimized structure and compare them with the experimental structure. The agreement is quite good, considering that only a partial geometry optimization was attempted. The calculated distances are slightly longer than the experimental ones; for this reason, the bending of the indenyl ligand is a bit smaller (17.5° vs experimental value of 21.4°), but the sequence of distances is maintained.

The dicationic species $[(\eta^5\text{-Ind})(Cp)MoL_2]^{2+}$ exhibit a different relative arrangement of the two rings, as discussed above. In the four complexes for which crystal structures have been determined (Table 4), the λ angle ranges from 93.5° (LEHXEB) to 117.1° ($\mathbf{1}^{2+}$). Under C_s symmetry, a local minimum was found, but after allowing the indenyl ligand to rotate 90° and then optimizing without any imposed symmetry, a new energy minimum was found at 12.3 kJ mol^{-1}. The most relevant structural parameters, shown in Figure 12a for the calculated structure of $[(\eta^5\text{-Ind})(Cp)Mo(CO)_2]^{2+}$ compare well with the structure of the related phosphite dicationic complex described above.

The complete rotation of the indenyl ligand in the two complexes of different charge was also studied using extended Hückel calculations. In $(\eta^3\text{-Ind})(Cp)Mo(CO)_2$, the energy varies by only small amounts; as λ is changed, indicating indenyl fluxionality, the staggered arrangement is the most stable, followed by the eclipsed. The electronically preferred[26] conformation that puts the six-membered ring above the two carbonyl groups, and leads to a better metal to CO back-donation, is not observed in these compounds for steric reasons. For $[(\eta^5\text{-Ind})(Cp)Mo(CO)_2]^{2+}$, the conformation having $\lambda = 90°$

(25) (a) Calhorda, M. J.; Gamelas, C. A.; Gonçalves, I. S.; Herdtweck, E.; Romão, C. C.; Veiros, L. F. *Organometallics* **1998**, *17*, 2597.

(26) Calhorda, M. J.; Veiros, L. F. *Coord. Chem. Rev.* **1999**, *185−186*, 37.

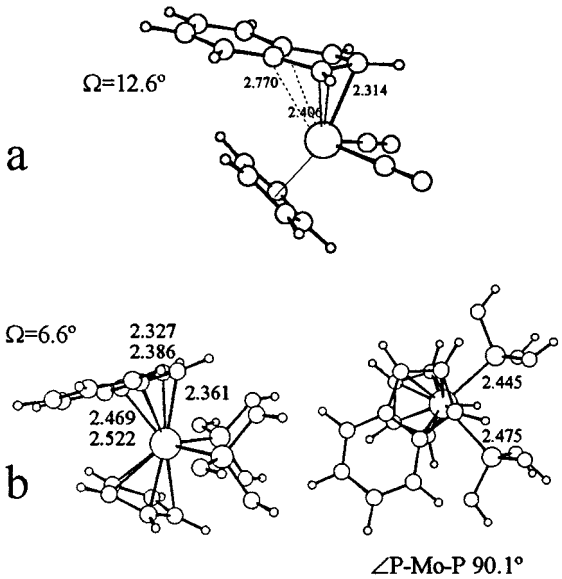

Figure 12. Structure of $[(\eta^5\text{-Ind})CpMo(L)_2]^{2+}$ complexes calculated with DFT. (a) L = CO. (b) L = $P(OH)_3$, side view (left) and top view (right).

has an energy 28.8 kJ mol^{-1} lower than that of the $\lambda = 0°$ conformer, in agreement with structural data.

Turning to phosphite complexes with L = $P(OH)_3$ in order to model **1** and its mono- and dications, full geometry optimizations were performed using DFT calculations without any symmetry constraints (Figures 11b and 12b). The calculated geometrical features are very similar to the data given above (Tables 3 and 4, and text) for complex **1**, $(\eta^3\text{-Ind})(Cp)\text{-}\{P(OMe)_3\}_2$. For example, the experimental folding angle of 21.7° is modeled well by the calculated angle of 22.0°. The same full geometry optimization was carried out for the dicationic phosphite complex. Again, the calculated geometry (Figure 12b) is very similar to that observed for $\mathbf{1}^{2+}$. The asymmetry between distances of the same kind is more pronounced, as no symmetry element is present in this structure. The two Mo−P distances differ by 0.03 Å. The five Mo−C distances to the five-membered ring of the indenyl are typical of η^5-Ind coordination, with the two distances to the hinge (junction) carbon atoms being longer. The fact that the calculated P−Mo−P angle is wider than the experimental value (90.1°, 86.9°) is probably due to the use of $P(OH)_3$ instead of $P(OMe)_3$ in the model (bulkier groups will increase the L−Cp repulsion).

A full geometry optimization was also performed on the monocation $[(\eta\text{-Ind})(Cp)Mo\{P(OH)_3\}_2]^+$. Considering that the orientation of the six-membered ring relative to the two L ligands of the complex is one of the distinguishing features between η^5 and η^3 coordination, we decided to optimize the geometry in the absence of symmetry. The result is shown in Figure 13.

The selected data shown in Figure 13 indicate that the coordination is intermediate *between* η^5 and η^3. Indeed, the indenyl ligand is folded by 11.4°, but the six-membered moiety still lies trans to the two $P(OH)_3$ ligands. In $(ring)_2ML_2$ complexes, $\lambda = 0°$ tends to be preferred, as it minimizes ring−L repulsion. However, a planar η^5-indenyl suffers strong repulsion from Cp, and $\lambda = 90°$ becomes favored. When the indenyl bends and moves away from the metal, the $\lambda = 0°$ conformation becomes clearly favorable. Notice that although the calculations were done in the absence of geometry constraints, there is a mirror plane in the structure. The Mo−C distances are 2.302 [C(2)], 2.410 [C(1) and C(3)], and 2.788 Å [C(4) and C(9)],

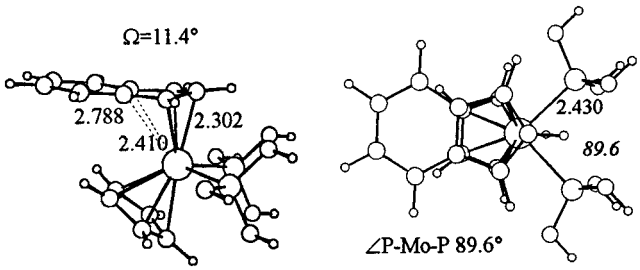

Figure 13. Structure of $[(\eta\text{-Ind})CpMo\{P(OH)_3\}_2]^+$ calculated with DFT, side view (left) and top view (right).

similar to those found for the carbonyl complex. One may expect that the P−Mo−P angle will be smaller, owing to the presence of $P(OH)_3$ ligands, as discussed above for the other complexes. The geometry of this complex can be compared to that of the formally 20-electron compound $(Ind)_2Ni$, assuming that each indenyl ring has acquired one extra electron, just as in our monocation, as has been discussed elsewhere.[25]

The other relevant question concerns the localization of the spin density. The DFT calculations indicate that the highest concentration of spin density resides in the molybdenum atom (0.70). Significant concentrations of spin density are also found on two carbons of the Cp ring (0.046 and 0.050) and the benzene carbons of the indenyl (0.044, 0.030, 0.057, 0.054, 0.032, 0.042), as well as on the isolated carbon C(2) in the mirror plane of the molecule (−0.017), and the phosphorus atoms (−0.010 and −0.011). The contributions of the other two carbons are negligible, as indeed are those of the other atoms.

Theoretical Studies: ESR Hyperfine Splittings. To aid in the interpretation of ESR hyperfine splittings (hfs) (vide ante) of the odd-electron complexes in this series, DFT calculations were performed using the ZORA formalism within the ADF program (see Experimental Section for details). The spin-unrestricted calculational method within this formalism has been shown to be an effective means of characterizing hyperfine splittings of transition metal complexes.[27]

Comparison of the calculated[28] and experimental hfs values of Mo and P were of less interest than the findings for H, because those of Mo and P are roughly as expected.[29] The predicted $a_{H(2)}$ values are highly informative, because the value for H(2) is predicted to be much larger than that of any other proton in $\mathbf{1}^+$. The calculated isotropic splitting, $a_{H(2)}$, of 6.7×10^{-4} cm^{-1} is in excellent agreement with the experimental value of 7.3×10^{-4} cm^{-1} for $\mathbf{1}^+$ and with the value of 7.5×10^{-4} cm^{-1} measured as the average for $\mathbf{1}^+$, $\mathbf{2}^+$, and $\mathbf{3}^-$. DFT theory accounts, therefore, for the apparent disagreement between the large measured proton hfs and the minimal SOMO spin densities (<6%) on any C−H carbon. A SOMO-restricted spin-polarization value would be less than about 1.5×10^{-4} cm^{-1} for any proton in these radicals. The greater unpaired spin density at hydrogen H(2) apparently arises from polarization of H(2) by lower, inner-occupied shells in addition to electron spin in the SOMO. This finding is in accord with the recent arguments of Braden and Tyler that such interactions are necessary to explain hyperfine splittings in many organometallic radicals.[22]

(27) Belanzoni, P.; Baerends, E. J.; Gribnau, M. *J. Phys. Chem. A* **1999**, *103*, 3732.

(28) Approximate isotropic hfs predicted for nuclei other than H(2) in complex $\mathbf{1}^+$: a_{Mo}, 8×10^{-4} cm^{-1}; a_{Pt}, 8×10^{-4} cm^{-1}; $a_{H(1)} = 0.7 \times 10^{-4}$ cm^{-1}; and $a_{H(3)} = 0.2 \times 10^{-4}$ cm^{-1}

(29) For leading references see: (a) Wang, L.−S.; Fettinger, J. C.; Poli, R.; Meunier-Prest, R. *Organometallics* **1998**, *17*, 2692. (b) Connelly, N. G.; Geiger, W. E.; Lovelace, S. R.; Metz, B.; Paget, T. J.; Winter, R. *Organometallics* **1999**, *18*, 3201. (c) Pierce, D. T.; Geiger, W. E. *Inorg. Chem.* **1994**, *33*, 373.

Table 5. Selected Literature Examples of Redox Processes Involving η^5/η^3 or η^6/η^4 Hapticity Changes

redox couples	$E_{1/2}(1) - E_{1/2}(2)$ in mV	lower k_s	change in η	radical	concerted?[a]	ref
$(Ind)Fe(CO)_3^{+/0/-}$	680	$k_s(2)$[b]	second redn	19 e^-	yes	4
$(Ind)_2V(CO)^{+/0/-}$	520	$k_s(1)$[b]	first redn	17 e^-	*c*	7
$(arene)CpRh^{2+/+/0}$	200−330[d]	$k_s(2)$	second redn	19 e^-	yes	30, 34
$(Ind)Rh(cod)^{0/-/2-}$	300	$k_s(1)$	first redn	17 e^-	no	9
$(Ind)Mn(CO)_3^{+/0/-}$	250	*e*	second redn	19 e^-	yes	8
$(C_6Me_6)_2Ru^{2+/+/0}$	∼0	$k_s(2)$	second redn	19 e^-	yes	13

[a] Concerted: concomitant structure change and electron transfer (E mechanism). [b] Heterogeneous electron-transfer rates were not reported, but a qualitative assessment was possible from the comparative CV peak separations. [c] The authors suggested a sequential (EC, square scheme) process, but voltammetric confirmation of the mechanism was not reported. [d] Dependent on the arene involved. [e] No information available; the two reduction waves had close to Nernstian shapes at slow scan rates.

Discussion

Because electrochemical data are frequently used to identify whether an η^5/η^3 or η^6/η^4 hapticity change occurs in the first or second step of an overall two-electron process, it is worthwhile to see how the present $\Delta E_{1/2}$ and k_s data compare with those reported in conceptually similar literature examples. References to many of the previous studies were given in the Introduction. When both one-electron waves are observed, one may attempt to make use of thermodynamic ($E_{1/2}$ values) or kinetic (k_s values) factors that may differ depending on whether the major structural change occurs in the first or second electron transfer process. It is generally thought that if the dominant structural change occurs concomitant with the *second* reduction process, the absolute values of $\Delta E_{1/2}$ will be smaller than if no structural reorganization occurs in either step[30] and the heterogeneous electron-transfer rate $k_s(2)$ will be considerably lower than $k_s(1)$.[18] One or the other of these guides has been employed in assigning 17-electron[9] or 19-electron[4,8] structures to metal−indenyl radicals, as well as to metal−arene radicals.[13,31] Some of the limitations of such models, especially when it is not firmly established whether the electron-transfer process and structural change are concomitant ("simple" E mechanism) or sequential (EC mechanism), have been discussed.[9,10] In the precedents collected in Table 5, we note the following: (i) for systems having apparently concomitant changes of structure with electron transfer,[7,8,13,31] if the value of $\Delta E_{1/2}$ is "small" (arbitrarily, less than 300 mV), the radical has been generally assigned (or demonstrated to have) a 19-electron structure (one exception is that of the iron complex $(Ind)Fe(CO)_3$, assigned a 19-electron structure although $\Delta E_{1/2}$ for the two one-electron reduction waves of $[(\eta^5\text{-Ind})Fe(CO)]^+$ is quite large (680 mV)),[4] and (ii) with the exception of $(Ind)_2V(CO)_2$,[6,7] a slower electron-transfer rate, when measured, has always been observed for the couple involving the assigned hapticity change.[4,9,13,31]

The $\Delta E_{1/2}$ values of point (i) are influenced by several factors *other than* structural changes, including electronic configurations as well as solvation and ion-pairing effects.[32] They should be used with appropriate caution when attempting to assign probable hapticity changes. Judgments based on different electron-transfer rates, relevant to point (ii) above, appear to have fewer caveats. Still, there is little information on precisely what k_s values are *expected* for electron-transfer induced hapticity changes of the type being discussed, because the inner-sphere reorganization energies,[33] λ_{in}, of these structural changes are not easily calculated. The simplest attempt to do so assumes that λ_{in} is equal to the changes in bond energy induced by the electron-transfer reaction.[34] In the present case, the lower k_s values for the slower $E_{1/2}(1)$ couples of **1**, **2**, and **3** suggest a range of 16.7−41.8 kJ/mol for λ_{in}. These are for the most part much lower than the values (38.5−77.0 kJ/mol) necessary to account for the η^6/η^4 changes in metal−arene complexes,[13,35,36] or that (∼54.4 kJ/mol) calculated from the k_s value reported for the reduction of (Ind)Rh(COD), **6**, which apparently involves an η^5/η^3 structural change.[9] Our electron-transfer rate data on complexes **1**−**3** are therefore qualitatively consistent with a model in which the structural change is likely greater in the Mo(IV)/Mo(III) couple, $E_{1/2}(1)$, than in the Mo(III)/Mo(II) couple, $E_{1/2}(2)$. The activation barriers for the $E_{1/2}(1)$ reactions appear, however, to be insufficient to account for a *complete* η^5/η^3 hapticity change in this single one-electron process. The DFT-calculated structure of $\mathbf{1}^+$ offers an explanation of this finding.

The odd-electron complex, $\mathbf{1}^+$, is determined to have three Mo−C bond lengths typical of π-bonding to the indenyl group (average ∼2.34 Å) and two Mo−C distances that are much longer (∼2.78 Å). The difference between these average distances, ΔMC, has been shown to be a useful gauge for defining the coordination and the "slippage" of an indenyl ligand, rising from about 0.1−0.2 Å for an η^5 complex to 0.6−0.7 Å for an η^3 complex.[24] The value calculated for $\mathbf{1}^+$, 0.44 Å, is about midway between these extremes. The calculated "fold" angle of the indenyl ligand (11.4°) is also between the average values reported for η^5 and η^3 indenyl complexes.[24,26] Specifically, it is about half the value (21.5°) observed for the true η^3 complexes, **1** and $(\eta^3\text{-Ind})(Cp)Mo(CO)_2$ (Table 4). For these reasons, the hapticity of the indenyl ring in $\mathbf{1}^+$ and, presumably, in isoelectronic complexes $\mathbf{2}^+$ and $\mathbf{3}^-$ is arguably *midway* between the idealized η^3 and η^5 shapes. It may be asserted that the Mo−indenyl bonding in the odd-electron species is closer to η^3, but with two additional weak bonds[37] to the C(4) and C(9) indenyl carbons that keep the indenyl ligand from completing its partial dissociation until another electron is added to the complex. In this sense, the metal−indenyl shapes of the odd-electron complexes are analogous to those of the bisindenyl complex $(Ind)_2Ni$ [5], in which the role of indenyl

(30) A geometric change concomitant with charge transfer energetically facilitates the product, leading to a less negative reduction potential; if restricted to the second reduction of an EE reduction sequence, $\Delta E_{1/2}$ is smaller than if no geometric change occurred. Geometric change exclusively in the first reduction step is, by similar reasoning, expected to increase $\Delta E_{1/2}$.

(31) Bowyer, W. J.; Geiger, W. E. *J. Electroanal. Chem.* **1988**, *239*, 253.

(32) Evans, D. H.; Lehmann, M. W. *Acta Chem. Scand.* **1999**, *53*, 765.

(33) The inner-sphere reorganization energy, λ_{in}, is related to the inner-sphere activation barrier, ΔG^*_{IS}, by the expression $\Delta G^*_{IS} = \lambda_{in}/4$.

(34) (a) Saveant, J. M. In *Advances in Electron-Transfer Chemistry*; Mariano, P. S., Ed.; JAI Press: New York, 1994; Vol 4, p 53. (b) Andrieux, C. P.; Robert, M.; Saveant, J. M. *J. Am. Chem. Soc.* **1995**, *117*, 9340 and references therein.

(35) See ref 31 and the following: Bowyer, W. J.; Merkert, J.; Geiger, W. E.; Rheingold, A. L. *Organometallics* **1989**, *8*, 191. Merkert, J.; Nielson, R. M.; Weaver, M. J.; Geiger, W. E. *J. Am. Chem. Soc.* **1989**, *111*, 7084.

(36) Nielson, R. M.; Weaver, M. *Organometallics* **1989**, *8*, 1636.

ligands as effective four-electron donors reduces the Ni electron count to 18.

In summary, the η^5-indenyl complexes $[(\eta^5\text{-Ind})(\text{Cp})\text{MoL}_2]^{2+}$, L = phosphine, phosphite, or $^1/_2$ dppe, undergo two closely spaced one-electron reductions to the corresponding monocationic and (η^3) neutral complexes. A combination of X-ray experiments and DFT calculations shows that the change from η^5 to η^3 hapticity in the Mo−indenyl interaction occurs incrementally, in the sequence shown left to right. The monocation radical has an intermediate hapticity which corresponds to effective four-electron donation due to an η^3 interaction in addition to two half-strength Mo−C bonds.

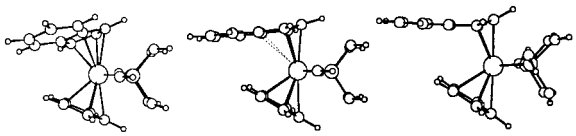

1^{2+} **1^{+}** **1**

Experimental Section

All experiments were carried out under an atmosphere of nitrogen by Schlenk techniques. Diethyl ether, THF, and pentane were dried by distillation from Na/benzophenone. Acetonitrile was dried over CaH_2 and distilled after refluxing several hours over CaH_2 or P_2O_5. Dichloromethane was distilled from CaH_2. Acetone was distilled and kept over 4 Å molecular sieves. Microanalysis measurements were performed by Mrs. Z. Tavares at the Instituto de Tecnologia Quimíca e Biológica, ITQB. ^{1}H NMR spectra were obtained with a Bruker AMX 300 spectrometer. Infrared spectra were recorded on a Unicam Mattson Mod 7000 FTIR spectrophotometer using KBr pellets. $[(\eta^5\text{-Ind})(\text{Cp})\text{Mo}(\text{CO})_2][\text{BF}_4]_2$, $[(\eta^5\text{-Ind})(\text{Cp})\text{Mo}(\text{NCMe})_2][\text{BF}_4]_2$,[14a] and $\text{Mo}(\eta^3\text{-}C_3H_5)\text{Cl}(\text{CO})_2(\text{NCMe})_2$[38] were prepared as described previously.

$[(\eta^5\text{-Ind})(\text{Cp})\text{Mo}(\text{P}(\text{OMe})_3)_2][\text{BF}_4]_2$ ($[1^{2+}]$ $[\text{BF}_4]_2$). A solution of $[(\eta^5\text{-Ind})(\text{Cp})\text{Mo}(\text{NCMe})_2][\text{BF}_4]_2$ (0.26 g, 0.50 mmol) in CH_2Cl_2/NMF (10/1) was allowed to react with excess $\text{P}(\text{OMe})_3$ (4 mL) for 2 h at room temperature. The resulting yellow solution was concentrated under vacuum until the only remaining solvent was NMF. Yellow crystals precipitated upon slow addition of Et_2O, in 80% yield. The complex was washed with CH_2Cl_2 and Et_2O. Anal. Calcd for $C_{20}H_{30}B_2F_2O_6P_2Mo$: C, 34.42, H, 4.33. Found: C, 34.50; H, 4.63%. Selected IR (KBr, cm^{-1}): 3399, 3090, 2957, 2847, 1537, 1486, 1300, 1055, 860, 785, 720, 559. ^{1}H NMR ($(CD_3)_2CO$, 300 MHz, rt, δ ppm): 7.93−7.90 (m, 2H, H(5−8)); 7.81−7.78 (m, 2H, H(5−8)); 6.35−6.32 (m, 2H, H(1/3)); 6.30−6.27 (m, 1H, H(2)); 5.82 (t, 5H, Cp, $^3J_{PH}$ = 2.1 Hz); 4.06 (t, 18H, $\text{P}(\text{OMe})_3$). ^{13}C NMR (CD_3CN, 75 MHz, rt, δ ppm): 134.4 (C(5/8)); 127.6 (C(6/7)); 112.4 (C(4/9)); 96.8 (Cp); 90.4 (C(2)); 88.2 (C(1/3)); 57.7 (CH_3).

The $[\text{BPh}_4]^-$ and $[\text{PF}_6]^-$ salts of $\mathbf{1}^{2+}$ were prepared by two successive counterion metathesis reactions as described in the Supporting Information.

(η^3-Ind)CpMo(P(OMe)$_3$)$_2$ (1). The addition of an NCMe solution of Cp_2Co (0.41 g, 2.19 mmol) to the complex $[(\eta^5\text{-Ind})(\text{Cp})\text{Mo}(\text{P}(\text{OMe})_3)_2][\text{BF}_4]_2$ (0.77 g, 1.10 mmol) dissolved in the same solvent caused the immediate change. After stirring for 2 h at room temperature, the solvent was removed under vacuum and the residue extracted with hexane (2 × 30 mL). Upon evaporation of the solvent, the orange crystalline product separated in 80% yield. Anal. Calcd for $C_{20}H_{30}O_6P_2Mo$: C, 45.81; H, 5.77. Found: C, 45.69; H, 5.88%. Selected IR (KBr, cm^{-1}): 3053, 2945, 2835, 1384, 1262, 1177, 1037, 748, 702. ^{1}H NMR (C_6D_6, 300 MHz, rt, δ ppm): 6.57−6.50 (m, 4H, H(5−8)); 4.58 (s, br, 5H, Cp, $^3J_{PH}$ = 5.4 Hz); 3.90−3.87 (m, 3H, H(1−3)); 3.24 (t, 18H, $\text{P}(\text{OMe})_3$). ^{13}C NMR (CH_3CN-d_3, 75 MHz, rt, δ ppm): 157.5 (C(4/9)); 120.2 (C(5/8)); 113.5 (C(6/7)); 95.8 (C(2)); 93.1 (Cp); 52.0 (CH_3).

The deutero derivative $[(1,3\text{-d-Ind})\text{CpMo}\{\text{P}(\text{OMe})_3\}_2][\text{BF}_4]_2$, [**d-1**]-$[\text{BF}_4]_2$, was prepared in the same fashion as its protio analogue beginning with a sample of 1,1,3-trideuterioindene as described in detail in the Supporting Information.[39] Three-fold repetition of the deuteration process and subsequent distillation yielded a 70%-deuterated sample of indene [quantitation by means of the integration of the ^{1}H NMR spectrum, namely of the vinylic singlet at δ = 6.59 ppm, attributed to H(2), relative to the triplet at δ = 3.38 ppm, attributed to the geminal protons H(1/1)]. NMR spectra were obtained with either 250 or 300 MHz spectrometers from Bruker. X-band ESR spectra were obtained on a Bruker ESP 300E spectrometer using 2,2-diphenyl-1-picrylhydrazyl (DPPH) as an external reference. Temperature control was achieved with a Bruker type B-VT unit down to 110 K. ESR spectra were simulated with a program (SpectSim) written by Prof. Philip Rieger of Brown University. All electrochemical experiments were performed under nitrogen within a Vacuum Atmospheres drybox which was outfitted with a cooling bath capable of controlling solution temperatures to better than 1 °C. Oxygen levels were typically 1−5 ppm over the course of an experiment. Solvents were distilled first under Schlenk and then under bulb-to-bulb high vacuum conditions. Care was taken to minimize both oxygen and trace water in all electrochemical experiments.[40]

Electrochemistry. A standard three-electrode configuration was employed for voltammetric and coulometric experiments. Although the experimental reference electrode was usually a AgCl-coated Ag wire, the potentials in this paper are referred to the ferrocene/ferrocenium couple (Fc). Either ferrocene or decamethylferrocene was added to the solution at an appropriate point to serve as an internal calibrant. The potential for decamethylferrocene is −0.553 V versus ferrocene in dichloromethane/0.1M tetrabutylammonium hexafluorophosphate. To convert the potentials in this paper to an SCE reference, 0.46 V must be added. Digital simulations of background-subtracted cyclic voltammograms were carried out using Digisim (Bioanalytical Systems, version 2.1); square wave voltammograms of the reduction of $\mathbf{1}^{2+}$ were simulated using the freeware application Electrochemical Simulations Package (ESP version 2.4). Analyte concentrations below 1 mM and working electrodes with radii of 2 mm or less served to minimize ohmic errors. Background charging currents were subtracted by recording CV scans over a range of scan rates on the solution containing only supporting electrolyte, before addition of the analyte. Other details of the electrochemical procedures have recently been described.[41]

Crystallography. The pertinent crystallographic data together with refinement details for complexes **1** and $\mathbf{1}^{2+}$ are given in Table 6. Crystal data for both complexes were collected with a MAR research image plate system using graphite-monochromated Mo Kα radiation (λ = 0.710 73 Å). The crystals were positioned at 70 mm from the image plate. 95 frames were measured at two degree intervals with a counting time of 3 min. Data analysis was carried out with the XDS program.[42] Intensities were not corrected for absorption effects. The positions of the molybdenum atoms were determined by direct methods, and the positions of remaining non-hydrogen atoms were obtained by successive difference Fourier synthesis. All hydrogen atoms were refined giving thermal parameters equivalent to 1.2 times those of the atoms to which they were bonded. Anisotropic temperature factors were used for all non-hydrogen atoms. The structures were refined by least-squares methods on F^2 until convergence was achieved. All calculations were carried out with SHELXS and SHELXL within the SHELX97 package.[43] Molecular diagrams were drawn with XPMA and ZORTEP programs.[44]

Theoretical Calculations. Extended Hückel calculations were carried out using the EH method[45] with modified H_{ij} values.[46] The basis

(37) The Mo−C(4) and Mo−C(5) distances ~2.78 Å are also considerably less than those (~3.055 Å) of another genuine η^3-indenyl ligand in the related complex (η^3-Ind)(η^5-Ind)Mo(dppe): Poli, R.; Mattamana, S. P.; Falvello, L. R. *Gazz. Chim. Ital.* **1992**, *122*, 315.

(38) Hayter, R. G. *J. Organomet. Chem.* **1968**, *13*, P1.
(39) (a) Bergson, G. *Acta Chem. Scand.* **1964**, *18*, 2003. (b) Willner, I.; Halpern, M.; Rabinovitz, M. *J. Chem. Soc., Chem. Commun.* **1978**, 155.
(40) Details are available: Stoll, M. E. Ph.D. Dissertation, University of Vermont, Burlington, VT, 2000.
(41) Stoll, M. E.; Lovelace, S. R.; Geiger, W. E.; Schimanke, H.; Hyla-Kryspin, I.; Gleiter, R. *J. Am. Chem. Soc.* **1999**, *121*, 9343.
(42) Kabsch, W. *J. Appl. Crystallogr.* **1988**, *21*, 916.
(43) (a) Sheldrick, G. M. SHELXS-86. *Acta Crystallogr.* **1990**, A46. (b) Sheldrick, G. M. *SHELX-97*; University of Göttingen: Göttingen, 1997.
(44) Zsolnai, L. *XPMA and ZORTEP*; University of Heidelberg: Heidelberg, 1994.

Table 6. Room Temperature Crystal Data and Refinement Details for Complexes **1** and $\mathbf{1}^{2+}$

	1	$\mathbf{1}^{2+}$
formula	$C_{20}H_{30}MoO_6P_2$	$C_{20}H_{30}B_2F_8MoO_6P_2$
M_r	524.32	697.94
crystal system	orthorhombic	monoclinic
space group	*Pbca*	$P2_1/n$
a/Å	8.621(11)	11.375(13)
b/Å	19.142(22)	12.471(15)
c/Å	27.504(31)	19.868(22)
β/(deg)	(90.0)	99.03(1)
V/Å^3	4539(9)	2783(6)
Z	8	4
D_c/g cm^{-3}	1.535	1.665
μ/mm^{-1}	0.752	0.674
F(000)	2160	1408
θ range/deg	2.69−25.82	2.23−25.93
index ranges *hkl*	$0 \le h \le 9$, $-23 \le k \le 23$, $-33 \le l \le 33$	$0 \le h \le 12$, $-15 \le k \le 15$, $-24 \le l \le 24$
reflections collected	14 511	7771
unique reflections	4034 ($R_{int} = 0.0332$)	4431 ($R_{int} = 0.0234$)
tefined parameters	268	359
goodness-of-fit on F	1.108	1.088
final R indices $[I > 2\sigma(I)]$		
R_1, wR_2[a]	0.0582, 0.1301	0.0551, 0.1589
R indices (all data)		
R_1, wR_2	0.0777, 0.1444	0.0747, 0.1776
largest diff peak and hole/e Å^{-3}	1.179 and −0.627	1.194 and −0.708

[a] $R_1 = \sum(||F_o| - |F_c||)/\sum|F_o|$; $wR_2 = [\sum w(F_o^2 - F_c^2)^2/\sum w(F_o^2)^2]^{1/2}$; $w \equiv 1/[\sigma^2(F_o^2) + (aP)^2 + bP]$, $P = [\max(F_o^2) + 2F_c^2]/3$.

set for the metal atoms consisted of n s, n p, and $(n-1)$ d orbitals. The s and p orbitals were described by single Slater-type wave functions, and the d orbitals were taken as contracted linear combinations of two Slater-type wave functions. The parameters used for Mo were (H_{ii} (eV), ζ): 5s, 8.77, 1.960; 5p, 5.60, 1.900; 4d, 11.06, 4.542, 1.901 (ζ_2), 0.5899 (C_1), 0.5899 (C_2). Standard parameters were used for other atoms. The program CACAO was used in calculations.[47]The calculations were performed on model complexes having geometries with C_s symmetry, taken from the experimental structures noted in the text. Thus, $[(\eta^m\text{-Ind})CpMo(CO)_2]^{n+}$ ($m = 3$, $n = 0$ or $m = 5$, $n = 2$) complexes have a distorted pseudotetrahedral geometry around the metal with Ind−Mo−Cp and CO−Mo−CO angles of 140° and 80°, respectively; the trihapto coordination mode of the indenyl ligand was accomplished by a $\Omega = 30°$ bending of that ligand. The bonding distances (Å) were as follows: M−(C_5 ring centroid), 2.00; M−C(CO), 2.00; C−O, 1.25; C−C, 1.40; C−H, 1.08.

Density functional calculations[48] were carried out on model compounds based on the structures of $\mathbf{1}^{2+}$ for the $[(\eta^5\text{-Ind})(Cp)Mo(CO)_2]^{2+}$ complex, without symmetry, and of **1**, under C_s symmetry, using the Amsterdam density functional (ADF) program[49]developed by Baerends and co-workers (release 2.3).[50] The slipping, folding, and position of the indenyl ring and the angles between the ligands (indenyl, Cp, CO) were optimized for the carbonyl complexes. Full optimization was carried out for the phosphite complexes. Vosko, Wilk, and Nusair's local exchange correction potential was used,[51] together with Becke's nonlocal exchange[52] and Perdew's correlation corrections.[53] Unrestricted calculations were performed for the paramagnetic complexes. The geometry optimization procedure was based on the method developed by Versluis and Ziegler,[54]using the nonlocal correction terms in the calculation of the gradients. The core orbitals were frozen for Mo ([1−3]s, [1−3]p, 3d) and C, N, O (1s). Triple ζ Slater-type orbitals (STOs) were used for H 1s, C, N, O 2s and 2p, and Mo 4s and 4p. A set of polarization functions was added: H (single ζ, 2p), C, N, O (single ζ, 3d). The ADF-1999 release was used to calculate the ESR parameters. An all valence basis set was used for all atoms, and spin−orbit coupling and relativistic effects were taken into account, within the "zeroth order relativistic approximation" ZORA formalism of ADF-1999.[49]

Acknowledgment. This work was supported by the National Science Foundation and by PRAXIS XXI. I.S.G. (BPD) and C.A.G. (BD) thank PRAXIS XXI for grants; V.F. thanks the British Council and FCT for funding. We also thank EPSRC (U.K.) and the University of Reading for funds for the Image Plate Systems, the National Science Foundation and University of Vermont for purchase of an ESR spectrometer, and Drs. Dale Braden and David Tyler for helpful correspondence on the ESR results.

Supporting Information Available: Frozen solution ESR spectrum of $\mathbf{1}^+$ (1 page, PDF). Text giving detailed procedures for the preparations of deuterated complexes (3 pages, PDF). This material is available free of charge via the Internet at http://pubs.acs.org.

JA0109951

(45) (a) Hoffmann, R. *J. Chem. Phys.* **1963**, *39*, 1397. (b) Hoffmann, R.; Lipscomb, W. N. *J. Chem. Phys.* **1962**, *36*, 2179.

(46) Ammeter, J. H.; Burgi, H.-J.; Thibeault, J. C.; Hoffmann, R. *J. Am. Chem. Soc.* **1978**, *100*, 3686.

(47) Mealli, C.; Proserpio, D. M. *J. Chem. Educ.* **1990**, *67*, 39.

(48) Parr, R. G.; Yang, W. *Density Functional Theory of Atoms and Molecules*; Oxford University Press: New York, 1989.

(49) (a) Baerends, E. J.; Bérces, A.; Bo, C.; Boerrigter, P. M.; Cavallo, L.; Deng, L.; Dickson, R. M.; Ellis, D. E.; Fan, L.; Fischer, T. H.; Fonseca Guerra, C.; van Gisbergen, S. J. A.; Groeneveld, J. A.; Gritsenko, O. V.; Harris, F. E.; van den Hoek, P.; Jacobsen, H.; van Kessel, G.; Kootstra, F.; van Lenthe, E.; Osinga, V. P.; Philipsen, P. H. T.; Post, D.; Pye, C. C.; Ravenek, W.; Ros, P.; Schipper, P. R. T.; Schreckenbach, G.; Snijders, J. G.; Sola, M.; Swerhone, D.; te Velde, G.; Vernooijs, P.; Versluis, L.; Visser, O.; van Wezenbeek, E.; Wiesenekker, G.; Wolff, S. K.; Woo, T. K.; Ziegler, T. *ADF*; 1999. (b) Fonseca Guerra, C.; Visser, O.; Snijders, J. G.; te Velde, G.; Baerends, E. J. Parallelisation of the Amsterdam Density Functional Programme. In *Methods and Techniques for Computational Chemistry*; Clementi, E., Corongiu, C., Eds.; STEF: Cagliari, 1995; p 303−395. (c) Fonseca Guerra, C.; Snijders, J. G.; te Velde, G.; Baerends, E. J. *Theor. Chem. Acc.* **1998**, *99*, 391.

(50) (a) Baerends, E. J.; Ellis, D.; Ros, P. *Chem. Phys.* **1973**, *2*, 41. (b) Baerends, E. J.; Ros, P. *Int. J. Quantum Chem.* **1978**, *S12*, 169. (c) Boerrigter, P. M.; te Velde, G.; Baerends, E. J. *Int. J. Quantum Chem.* **1988**, *33*, 87. (d) te Velde, G.; Baerends, E. J. *J. Comput. Phys.* **1992**, *99*, 84.

(51) Vosko, S. H.; Wilk, L.; Nusair, M. *Can. J. Phys.* **1980**, *58*, 1200.

(52) Becke, A. D. *J. Chem. Phys.* **1987**, *88*, 1053.

(53) (a) Perdew, J. P. *Phys. Rev.* **1986**, *B33*, 8822. (b) Perdew, J. P. *Phys. Rev.* **1986**, *B34*, 7406.

(54) (a) Versluis, L.; Ziegler, T. *J. Chem. Phys.* **1988**, *88*, 322. (b) Fan, L.; Ziegler, T. *J. Chem. Phys.* **1991**, *95*, 7401.

(55) Hostetler, M. J.; Butts, M. D.; Bergman, R. G. *Inorg. Chim. Acta* **1992**, *198*, 377.